ACS NANO
www.acsnano.org

Separation of Halogen Atoms by Sodium from Dehalogenative Reactions on a Au(111) Surface

Zhaoyu Zhang, Yuhong Gao, Zewei Yi, Chi Zhang,* and Wei Xu*

Cite This: *ACS Nano* 2024, 18, 9082−9091

Read Online

ACCESS | Metrics & More | Article Recommendations | Supporting Information

ABSTRACT: On-surface dehalogenative reactions have been promising in the construction of nanostructures with diverse morphologies and intriguing electronic properties, while halogen (X), as the main byproduct, often impedes the formation of extended nanostructures and property characterization, and the reaction usually requires high C−X activation temperatures, especially on relatively inert Au(111). Enormous efforts in precursor design, halogen-to-halide conversion, and the introduction of extrinsic metal atoms have been devoted to either eliminating dissociated halogens or reducing reaction barriers. However, it is still challenging to separate halogens from molecular systems while facilitating C−X activation under mild conditions. Herein, a versatile halogen separation strategy has been developed based on the introduction of extrinsic sodium (Na) into dehalogenative reactions on Au(111) as model systems that both isolates the dissociated halogens and facilitates the C−Br activation under mild conditions. Moreover, the combination of scanning tunneling microscopy imaging and density functional theory calculations reveals the formation of sodium halides (NaX) from halogens in these separation processes as well as the reduction in reaction temperatures and barriers, demonstrating the versatility of extrinsic sodium as an effective "cleaner" and "dehalogenator" of surface halogens. Our study demonstrates a valuable strategy to facilitate the on-surface dehalogenative reactions, which will assist in the precise fabrication of low-dimensional carbon nanostructures.

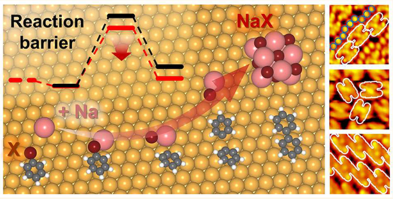

KEYWORDS: *on-surface synthesis, C−Br activation, dehalogenative reaction, scanning tunneling microscopy, density functional theory*

On-surface synthesis has shown great promise in fabricating low-dimensional nanostructures with atomic precision for potential molecule-based electronics, such as graphene nanoribbons and other carbon-based nanostructures.[1−5] Among various on-surface reactions, an Ullmann-type dehalogenative coupling reaction, as the most widely used one, has successfully constructed carbon nanostructures with diverse morphologies and intriguing electronic properties.[6−8] Despite the predesigned and well-controlled reaction manner, dehalogenative coupling reactions suffer from surrounding halogen obstacles, prohibiting the construction of extended carbon nanostructures and the property characterization,[9−11] as well as high activation temperatures accompanied by the desorption of precursors especially on inert Au(111). Accordingly, enormous efforts have been devoted to the elimination of dissociated halogens and the reduction of reaction barriers. Precursors with larger molecular weight were applied to avoid desorption, and samples were generally annealed at high temperatures to reduce halogens.[10−12] Moreover, converting halogens to halides with a low adsorption energy is another strategy. Specifically, H_2 and Si have been proved to be effective surface dehalogenators to form HBr and $SiBr_4$ from Br, respectively, followed by desorption,[13−15] which still requires harsh reaction conditions (typically high pressure, i.e., in the range of 10^{-7} mbar, and high substrate temperatures)[15,16] with possible quenching of reactive radicals in the former case and produces 1,4-disilabenzene (C_4Si_2) linkers (embedded in the molecular structures) in the latter.[17] On the other hand, the introduction of extrinsic metal atoms, e.g., Cu,[18] Pd,[19] Ni,[20] and Dy,[21] is an intriguing catalytic approach to lower the reaction temperatures of C−Br activation, with dissociated halogens still remaining and metal atoms strongly embedded in the organometallic structures. However, it remains a great challenge to eliminate the negative impacts of halogens, while facilitating C−Br activation under mild conditions. Therefore, it is of general interest to develop an alternative strategy to both activate the C−Br bonds and isolate the

Received: December 22, 2023
Revised: February 27, 2024
Accepted: March 5, 2024
Published: March 11, 2024

https://doi.org/10.1021/acsnano.3c12949
ACS Nano 2024, 18, 9082−9091

Scheme 1. Schematic Illustration Showing the Comparison between the Na-Facilitated Halogen Separation Strategy Demonstrated in This Study and the Conventional Na-Free Dehalogenative Reaction[a]

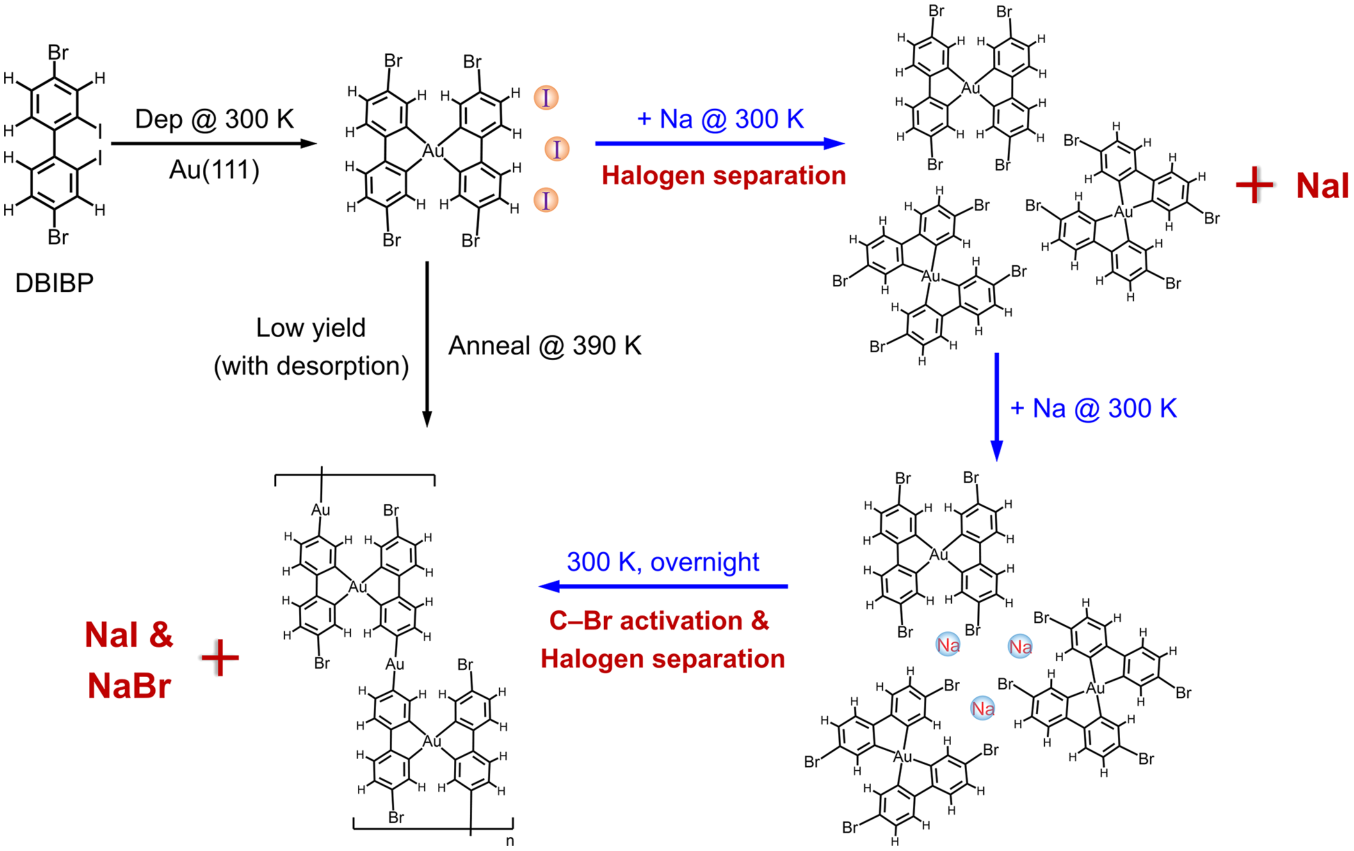

[a] Indicated by blue and black arrows, respectively.

dissociated halogens from target carbon-based nanostructures, which should be significant for structure construction with atomic precision and accurate property characterization.

In this study, a halogen separation strategy is developed by introducing extrinsic sodium (Na) into dehalogenative reactions on a Au(111) surface, which not only isolates the intermolecular dissociated halogens but also facilitates the intramolecular C−Br activation under mild conditions. As a model system, 4,4′-dibromo-2,2′-diiodo-1,1′-biphenyl (DBIBP), containing both Br and I substituents, was selected as the molecular precursor (Scheme 1). By a combination of high-resolution scanning tunneling microscopy (STM) imaging and density functional theory (DFT) calculations, Na-induced halogen separation processes on Au(111) have been visualized and evidenced to lead to the progressive structural transformation and subsequent construction of Na-interlinked intermediate structures, followed by further formation of coupled structures via C−Br activation at room temperature (RT, ∼300 K), which were also accompanied by the formation of NaX (X = halogen) islands (Scheme 1). In addition, the universality of this separation strategy was also validated in both aspects, using a more general molecule, 4,4″-dibromo-1,1′:4′,1″-terphenyl (DBTP). Furthermore, DFT calculations reveal that the reaction barriers for C−Br activation are generally reduced in the presence of Na, and more importantly, the combination of Na with halogens (forming NaX) separates dissociated halogens from the corresponding reaction systems, resulting in energetically more favorable situations compared to the Na-free cases. This study provides an effective strategy to steer the programmable dehalogenative reactions, which should benefit the construction of low-dimensional carbon-based nanostructures.

RESULTS AND DISCUSSION

After deposition of the DBIBP molecule on Au(111) held at ∼300 K, large islands composed of H-shaped motifs (shortened as H-motifs) formed (Figure 1a). The close-up STM image (Figure 1b) shows that H-motifs (as depicted by white contours) are densely aligned in a row surrounded by inter-row bright dots (indicated by blue circles), which further expand into molecular islands. In addition, each H-motif is composed of two bent rods as “legs” connected by a large bright dot at the center, and each end of the legs is decorated with a dot. Based on the submolecularly resolved STM image, an organometallic dimer structure[22] with a Au adatom linking two molecular components via C−Au contacts was calculated. The DFT-optimized structural model (left and bottom panels of Figure 1c) shows that two DBIBP molecules are connected via a Au adatom located in the bay region by forming four C−Au contacts as a result of deiodination,[23,24] while four Br substituents remain in the termini, in good agreement with the hierarchical dehalogenation scenario as reported.[25−27] Accordingly, the STM simulation (right) successfully reproduces the experimental topography. The small bright dots around the H-motifs are thus assigned to the dissociated iodine atoms. In this way, the deiodination took place with the formation of H-motifs and the generation of free intermolecular halogens,

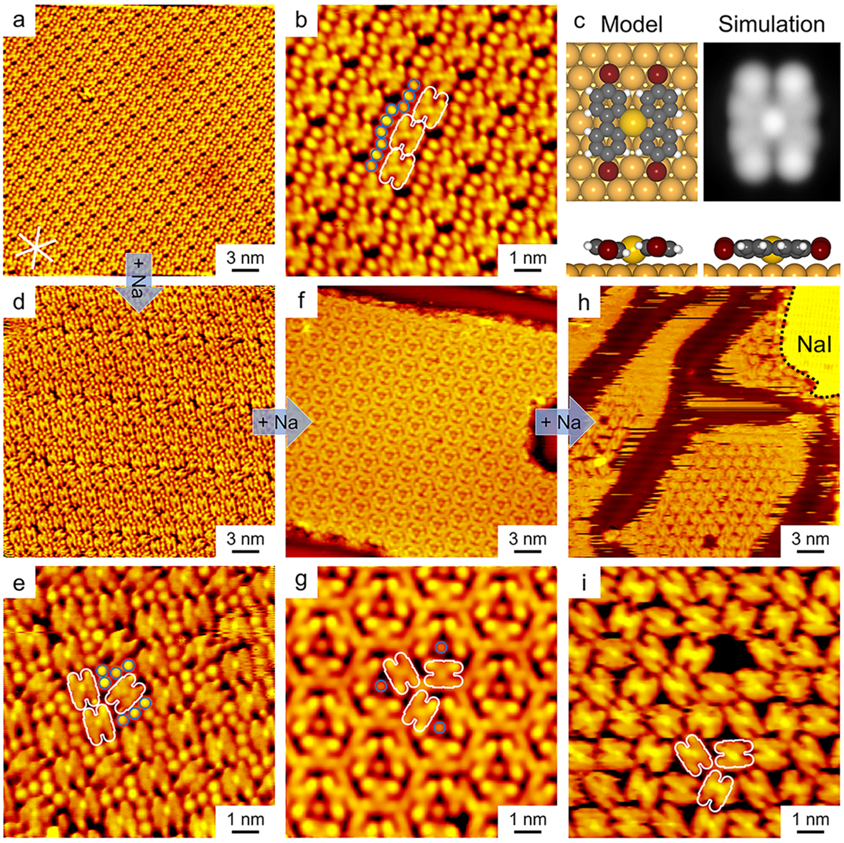

Figure 1. Gradual iodine separation from self-assembled molecular structures induced by Na on Au(111) at ∼300 K. (a, d, f, h) Large-scale and (b, e, g, i) close-up STM images showing the gradual structural transformation with reduced adjacent iodine atoms, induced by progressive deposition of Na at ∼300 K. The individual H-shaped motifs and iodine atoms are depicted by the white contours and blue circles, respectively. (c) Top and two side views of the DFT-calculated structural model and corresponding STM simulation (top right) of the H-motif: C, gray; H, white; Br, brown; Au, yellow. Scanning conditions: $V = -1.2$ V and $I = 0.7$ nA. The close-packed directions are illustrated as white lines in (a). The boundary of the NaI island is highlighted in black dotted lines in (h). The STM images were recorded in a typical temperature range of 100−150 K.

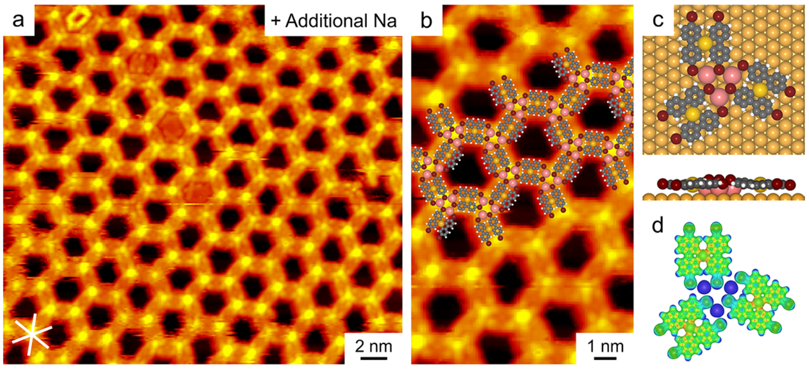

Figure 2. Construction of Na-interlinked metal−organic intermediate nanostructure by dosing additional Na at ∼300 K. (a) Large-scale STM image of 2D honeycomb metal−organic nanostructure. (b) Close-up STM image partially superimposed with the DFT-optimized molecular network. Scanning conditions: $V = -1.2$ V and $I = 0.7$ nA. The STM images were recorded in a typical temperature range of 100−150 K. (c) Top and side views of the DFT-calculated model of a Na-interlinked H_3Na_3 motif on Au(111): C, gray; H, white; Br, brown; Na, pink; Au, yellow. (d) Electrostatic potential map of the H_3Na_3 motif (the substrate was omitted for clarity), where blue and red represent positive and negative potential regions, respectively. The close-packed directions are indicated in (a).

which provides a model system to verify the feasibility of introducing Na to separate halogens.

Subsequently, pure Na atoms were dosed to the above sample held at ∼300 K, leading to an obvious phase transition (Figure 1d). From the close-up STM image (Figure 1e), individual H-motifs with decreased numbers of surrounding halogens could be clearly identified. By providing more Na (see Methods for more details) to the above sample in a controlled manner, further phase transition with decreasing halogens occurred (Figure 1f), where the stoichiometric ratio of halogens/H-motifs varied from ∼3:1 (Figure 1a,b), through ∼13:6 (Figure 1d,e), to ∼1:3 (Figure 1f,g). The zoomed-in

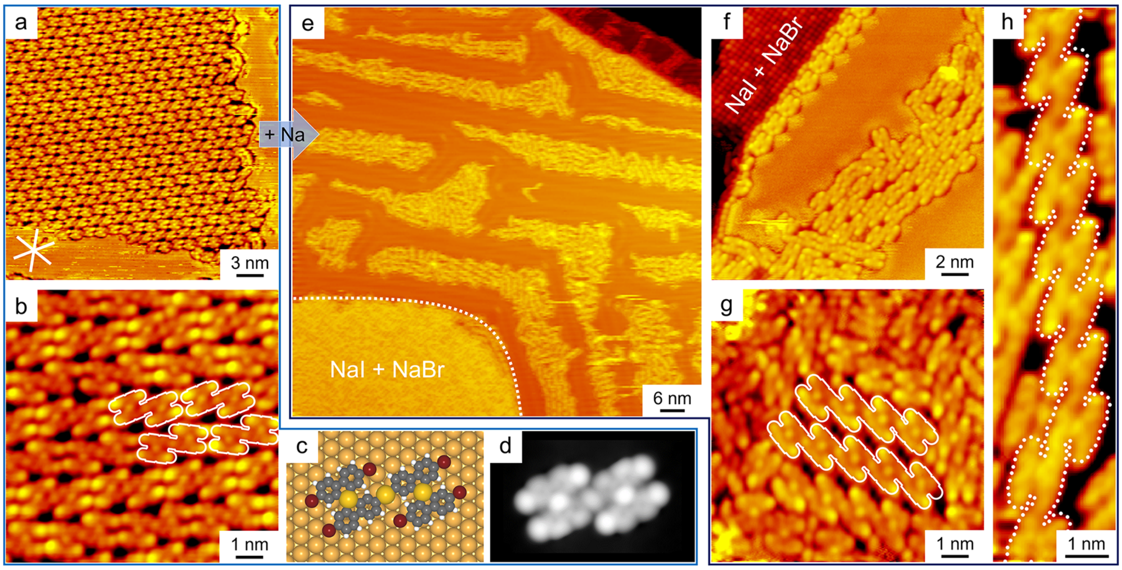

Figure 3. Further dehalogenative coupling with the formation of organometallic oligomers and NaX islands induced by Na at ∼300 K. (a) Large-scale and (b) close-up STM images showing the formation of molecular islands composed of H-based organometallic dimers, as typically depicted by the white contours. (c) DFT-optimized model and (d) simulated STM image of an H-motif on Au(111): C, gray; H, white; Br, brown; Au, yellow. (e) Large-scale and (f) close-up STM images showing the coexistence of molecular islands consisting of H-based organometallic oligomers and isolated NaX islands. (g) Magnified STM image showing more details of H-based organometallic oligomers (depicted by the white contours). (h) High-resolution STM image of an individual H-based chain highlighted in the white contour. The close-packed directions are indicated in (a). Scanning conditions: $V = -1.2$ V, $I = 0.5$ nA, and $T = 100-150$ K.

STM image (Figure 1g) shows that three highlighted neighboring H-motifs form a chiral triangle mainly via halogen bonds,[28,29] surrounded by three halogens at hydrogen-rich sites.[30,31] Interestingly, after successive deposition of Na atoms, the remaining halogens were thoroughly isolated from the molecular structures (Figure 1h,i), and small patches of H-motifs formed with molecules in a fuzzy state under scanning conditions due to the absence of intermolecular stabilizing halogens and the formation of weak intermolecular interactions (halogen bonds and C−H···Br interactions)[32] within H-motifs (Figure S1). Notably, during the introduction of Na atoms, the transformation of the assembled structures of H-motifs was accompanied by this gradual decreasing process of halogens until their complete isolation to form NaI salt islands (as shown in Figure 1h and detailed in Figure S2), revealing that the strong electrostatic interactions between Na and halogen atoms (i.e., I in this case) was the driving force for the successful isolation of halogens from molecular structures and thus the molecular structural evolution.[33] Hence, gradual intermolecular halogen isolation was realized by Na addition, leading to the separation of released halogens from molecular structures.

It is known that halogens are able to stabilize molecular structures via electrostatic interactions, as also shown above, but are generally obstacles to further coupling processes.[11,34] Inspired by our recent studies[33,35,36] and previous reports on extrinsic metal atoms,[18−21] additional Na atoms were introduced into the above sample to test the possibility of promoting the dehalogenative reactions. Upon further deposition of Na at ∼300 K, a two-dimensional (2D) honeycomb network structure was obtained (Figure 2a). From the close-up STM image, more details of the structure could be recognized (Figure 2b), where each side of the six-membered rings consists of an H-motif with less uniform bright junctions, which are presumably caused by the involvement of Na. In addition, the relative positions of three H-motifs in the Na-interlinked metal−organic clusters are not exactly the same, indicating different interaction modes between Na atoms and H-motifs. Based on the typical features and previous reports,[37,38] the involvement of excess Na in the assembled structure was proposed, and the corresponding DFT calculations on the structural models and STM simulations were performed (Figure S3). Accordingly, these bright dots at the junctions could be attributed to three, four, or even more Na atoms[35] interacting with Br substituents of H-motifs in different interaction modes. The model of a typical H_3Na_3 motif is shown in Figure 2c, in which each Na interacts with three Br substituents via electrostatic interactions. The corresponding network structure was thus tentatively superimposed on the zoomed-in STM image (Figure 2b), showing good agreement with the local part of the network. Moreover, the electrostatic potential map of the typical H_3Na_3 motif (Figure 2d) shows that the Na atoms are positively charged, while negative potential regions exist around the C−Br bond axes, which rationalizes the electrostatic interactions between Na atoms and the surrounding Br substituents at the side position and accords well with a recent report regarding the interaction between K and three Cl substituents.[37]

After the construction of the Na-interlinked metal−organic nanostructure, such a sample was then kept at ∼300 K for approximately 10 h. Interestingly, islands of a well-ordered, densely packed nanostructure appeared with no more bright junctions inside, as shown in the large-scale STM image (Figure 3a), indicating an apparent phase transition. The submolecularly resolved STM image (Figure 3b) displays that the nanostructure is composed of dimers, i.e., the connection of two H-motifs, as indicated by the white contours. Such dimers of the same chirality are aligned in one row with those of the opposite chirality in the adjacent row, forming islands in an alternating arrangement. A closer inspection reveals that

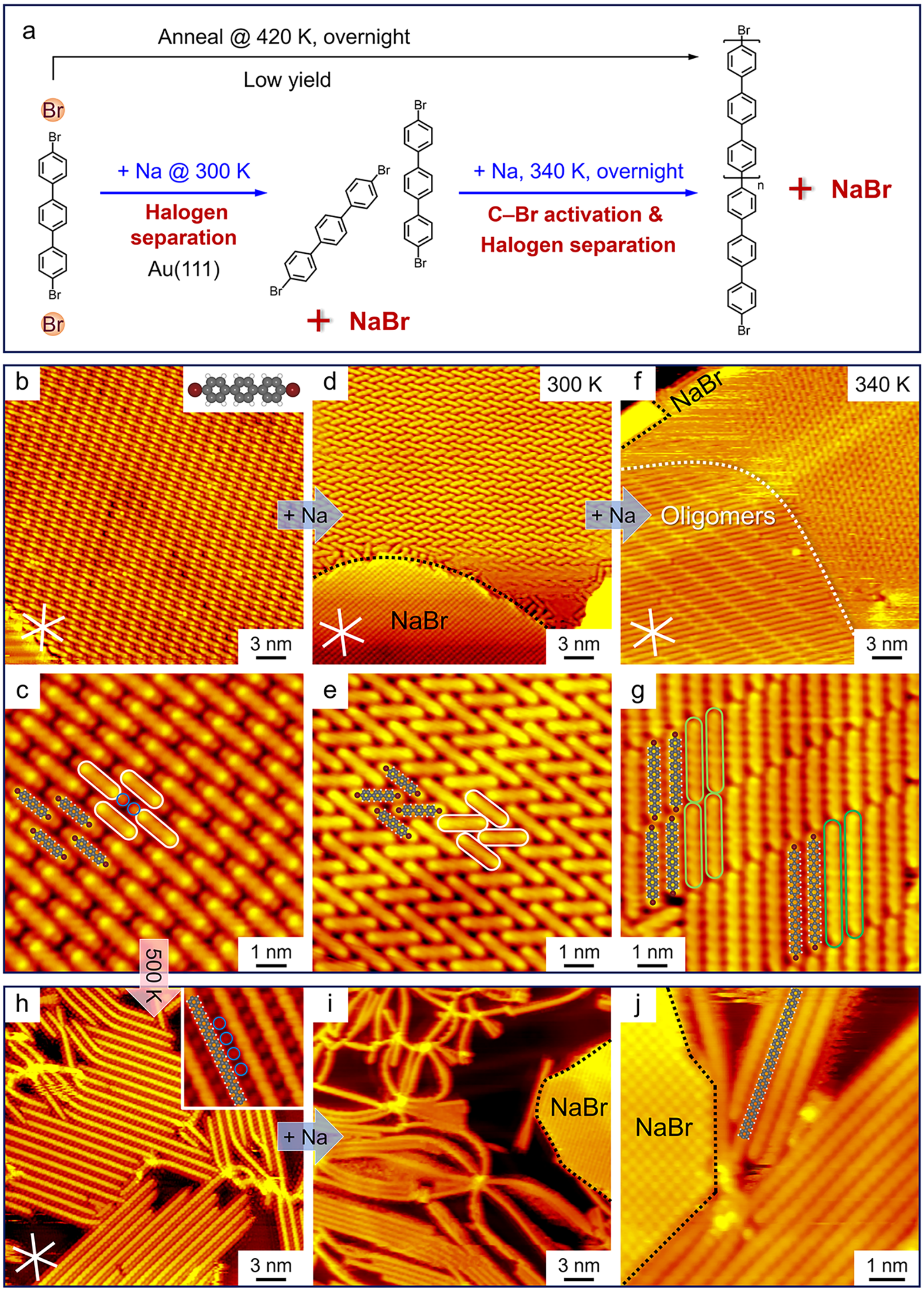

Figure 4. Na-induced halogen separation in the DBTP system on Au(111). (a) Schematic illustration showing the Na-facilitated halogen separation process and the Na-free process indicated by blue and black arrows, respectively. (b, d) Large-scale and (c, e) close-up STM images showing the structural transformation from (b, c) DBTP self-assembled structures coexisting with residual Br atoms to (d, e) pure DBTP islands and NaBr islands (separated by the black dotted line) after progressive Na deposition at ∼300 K. Inset of (b): the structural model of DBTP. The individual DBTP molecules are typically depicted by white rod-shaped contours and superimposed with models, and Br atoms are indicated by blue circles. (f) Large-scale and (g) close-up STM images showing the formation of molecular islands composed of DBTP-based oligomers, with remaining DBTP molecules and NaBr islands after further deposition of Na and annealing at ∼340 K for ∼10 h. (h) Large-scale STM image showing the formation of long polyphenylene chains with dissociated interchain Br atoms after annealing the DBTP-precovered sample at ∼500 K for 10 min. Inset: magnified STM image (size: 4 nm × 4 nm) overlaid with the structural model of a polyphenylene chain. (i) Large-scale and (j) close-up STM images showing the separation of polyphenylene chains and NaBr islands (with the boundaries highlighted in black dotted lines) after dosing Na at ∼300 K. The close-packed directions are indicated in white lines. Scanning conditions: $V = -1.2$ V, $I = 0.5$ nA, and $T = 100-150$ K.

two H-motifs are linked together by sharing one dot at the joint, which could be attributed to the dissociation of two terminal Br atoms and the addition of a Au adatom.[39] Then, DFT calculations on the dimer structure and the corresponding STM simulation were performed (Figure 3c,d), which successfully reproduced the typical STM morphology. In addition, the distance of the C−Au−C bond was measured to be ∼3.7 ± 0.2 Å from the STM image (Figure S4), which is comparable to those obtained in both the DFT calculations (4.1 Å) and a previous report (3−4 Å)[39] and is too long to be a covalent C−C bond. It is worth noting that free Au adatoms are usually not involved in the organometallic intermediates in the Ullmann-type coupling reactions on Au(111) but are embedded herein,[40] which is probably due to the steric hindrance caused by the staggered adsorption configuration of such an H-motif (see the side view in Figure 1c), similar to previous reports.[39,41] Moreover, the Au adatom located at the junction of two H-motifs appears to be darker than those at the center of the H-motif (Figure 3b), suggesting stronger bonding of the bay-region C_{aryl}−metal in a tetrabonding mode than that of a single C_{aryl}−metal−C_{aryl} one. Meanwhile, the termini of the other joint sides are lifted away from the surface (Figure S5), generally resulting in lower activity,[42] which rationalizes the dominance of the single-sided coupling. Therefore, with the assistance of excess Na, C−Br activation was validated to be feasible at RT.

Upon deposition of additional Na, these large well-ordered assembled islands (Figure 3a) were found to further break up into small molecular islands, and isolated salt islands (labeled NaI and NaBr) could also be clearly distinguished from these molecular islands (Figure 3e). The typical close-up STM image (Figure 3f) provides more details that the molecular islands are composed of organometallic oligomers with the NaX island isolated (where I and Br atoms appear as protrusions of different brightness). A further magnified STM image (Figure 3g) shows that H-based oligomers (as typically indicated by the white contours) are densely packed in the islands, and each oligomer is formed by "single-leg" coupled H-motifs through Au adatoms. In particular, a long chain with multiple H-motifs is shown in Figure 3h. It is noteworthy that due to the separation of halogens in the form of NaX islands from molecular structures, the recovery of herringbone reconstructions of the Au(111) surface could be clearly observed from the large-scale STM images (Figure S6 and Figure 3e), verifying the cleanness of blank areas, which is distinct from the situation of the halogen-covered samples without the participation of Na.

Furthermore, to experimentally discriminate the role of Na in the reaction process, a Na-free control experiment was carried out (Figure S7). After the sample precovered with H-motifs was annealed at ∼360 K, no change was observed (Figure S7a). Only when the annealing temperature reached ∼390 K did organometallic dimers form, surrounded by dissociated halogens (Figure S7b). Further increase of the annealing temperature to ∼410 K resulted in the construction of organometallic oligomers, unfortunately accompanied by the desorption of most of the molecules (Figure S7c). Consequently, it is concluded that the presence of Na promoted the dehalogenative coupling of H-motifs without affecting the product structures and, more importantly, contributed to the separation of halogens from the molecular structures.

In an attempt to explore the universality of the role of Na in the dehalogenative reactions, a simplified molecule, DBTP (Figure 4a), which has only one type of functional group (C_{aryl}−Br) as a typical Ullmann-type precursor and, more importantly, has been extensively reported with a rich database for direct comparison with our experiments, was selected as a more general molecular precursor for the model system. After deposition of DBTP on Au(111) held at ∼300 K, large molecular islands were observed (Figure 4b), consisting of intact DBTP molecules (depicted by white rod-shaped contours and superimposed with structural models, as shown in Figure 4c). Meanwhile, residual Br atoms (depicted by blue circles), which were deliberately introduced to verify the feasibility of separating free halogen atoms from this molecular system, were found to coexist at a DBTP/Br stoichiometric ratio of ∼1:2, providing the opportunity to demonstrate the role of extrinsic Na in the isolation of intermolecular halogens in a more general case. Also note that without the introduction of residual Br atoms, two kinds of self-assembled molecular structures were obtained after deposition of pure DBTP molecules onto Au(111) (see Figure S8 and detailed discussions in the Supporting Information). Accordingly, Na was gradually dosed to such a "DBTP + Br" sample kept at ∼300 K, and separation of pure DBTP islands (with a crossed self-assembled arrangement, which is identical to that of pure DBTP molecules upon deposition; see Figure S8) and salt (NaBr) islands was achieved (Figure 4d). From the close-up STM image (Figure 4e), it is unambiguously seen that Br atoms were thoroughly separated from DBTP islands, resulting in an obvious structural transformation, while the morphology of individual molecules remained the same. Hence, the Na-induced separation strategy for intermolecular halogens was generally validated as effective. Subsequently, more Na atoms were dosed, the sample was annealed at ∼340 K for ∼10 h, and interestingly, two distinct separate structures could be identified (with the boundary represented by the white dotted line), coexisting with NaBr islands (Figure 4f). A large number of islands composed of longer molecular rods appeared, while halogen-free crossed DBTP islands remained the same (see the upper right island). The magnified STM image (Figure 4g) further shows that the newly generated close-packed molecular structures are attributed to the DBTP-based oligomers, dominantly C−C coupled dimers and trimers (as depicted by the light and dark green contours and overlaid with the corresponding structural models, respectively), indicating the occurrence of dehalogenative coupling at quite low temperatures (∼340 K) on Au(111) in the presence of Na atoms in a general case.

Notably, a Na-free control experiment was also conducted, where no change was observed under the same condition, and after further annealing the DBTP-precovered Au(111) sample at ∼420 K for ∼10 h, only a small number of dimers appeared that coassembled with intact ones and were separated by inter-row Br atoms (Figure S9), distinct from the Na-involved situation. In addition, long polyphenylene chains with numerous Br atoms coexisting between the chains (highlighted by blue circles in the inset) were obtained only after annealing such a sample at ∼500 K for 10 min (Figure 4h). A similar trick was played again by dosing Na to the sample at ∼300 K, and the polyphenylene chains turned out to be tightly packed with a decreased interchain distance, while NaBr salt islands were generated away from the molecular structures (Figure 4i,j), further verifying the feasibility of the intermolecular halogen separation even from long chains. Note that to further provide experimental evidence for the formation and assign-

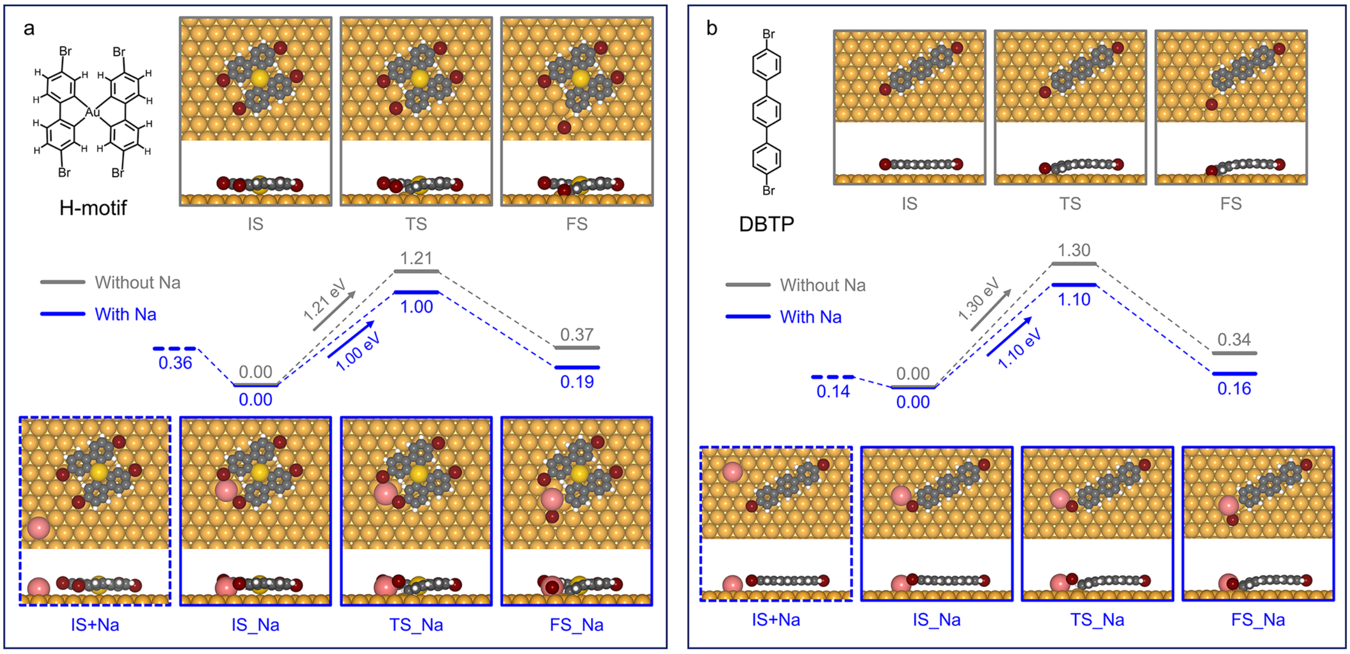

Figure 5. Reaction pathways for the C−Br activation of (a) H-motif and (b) DBTP molecule on Au(111) without (top panels) and with the assistance of Na (bottom panels), respectively. Structural models and energies of the initial states (IS), final states (FS), and transition states (TS) along the respective reaction pathways and the coexistence of the target molecule and Na without interaction (IS+Na) are given in units of eV with respect to the corresponding IS.

ment of NaI and NaBr islands after deposition of pure Na atoms onto the corresponding dehalogenative systems on Au(111) (via the separation of dissociated halogen atoms), we directly deposited the corresponding salts (NaI and NaBr) on Au(111) and compared their differences in morphologies and periodicities (Figure S10), which are found to be in good agreement with each other and with the reported values. Therefore, the halogen separation strategy by introducing extrinsic sodium onto Au(111) has been demonstrated in general cases.

To further reveal the role of Na, the debromination pathways of both the H-motif and the DBTP molecule were calculated using the DFT-based transition-state search, as shown in Figure 5. For the H-motif adsorbed on Au(111), one "leg" of each side is closer to the substrate due to the steric hindrance, as can be seen from the side view of the initial state (IS) in Figure 5a, resulting in easier debromination[42] and consequently formation of "single-leg" coupled products. In the absence of Na, the energy barrier of debromination was calculated to be ∼1.21 eV, and the debrominated product (FS) was energetically less stable than the IS by ∼0.37 eV, indicating that the debromination is an endothermic process. Upon the introduction of Na (cf. the bottom row in Figure 5a), IS+Na (H-motif) with the Na atom isolated is energetically less favorable (0.36 eV with respect to IS_Na), until the Na meets with the H-motif and stays between two Br substituents (IS_Na, 0 eV) via electrostatic interactions,[37,38] which is also consistent with the interactions within the honeycomb structures. With the assistance of Na, the Br atom from the H-motif is attracted to the Na atom (TS_Na) and then thoroughly bonded to it, and meanwhile, the debrominated H-motif-based radical directly interacts with the underlying substrate in a bent-down configuration, similar to the situation of the Na-free FS. Consequently, the Na-supported debromination barrier was reduced to 1.00 eV. In addition, the FS_Na (H-motif) was calculated to be more stable than IS+Na (H-motif), yet less stable than IS_Na (H-motif) by ∼0.19 eV. It is also noteworthy that the coexistence of H-based organometallic oligomers or chains and NaX salt islands was experimentally observed, indicating the diffusion and aggregation of NaX into islands at RT. Accordingly, we believe that the energy released in the diffusion and aggregation process of NaX into salt islands should be high enough to compensate for the energy deficit in the dehalogenative reactions (obtained by the reaction-pathway calculations), while such an exothermic formation process of salt islands could not be properly taken into account by DFT calculations. More importantly, the combination of Na with halogens separated free halogen atoms from the reaction systems, leading to the reaction equilibrium shift to the coupling side, especially for the reversible Ullmann reaction on Au(111).[43] Therefore, the participation of Na atoms was revealed to facilitate the reaction not only in reducing the reaction barrier but also in regulating the reaction equilibrium.

As an extension of a more general case, the debromination processes of the DBTP molecule both with and without the Na atom were calculated and are shown in Figure 5b. Similarly, the Na atom promoted the debromination process by lowering the reaction barrier from ∼1.30 to ∼1.10 eV, as well as by stabilizing the reaction product, confirming the universality of the halogen separation scenario of Na atoms. Moreover, the Au(111) surface is a nice balance among catalytic activity, molecular mobility, and relatively weak adsorption energy for radicals in C−X activation. The Au−Br and Au−C signals were observed in XPS experiments with the cleavage of C−Br bonds as a function of annealing temperatures in several dehalogenative systems on Au(111),[11,43,44] indicating the important role of Au(111). At the same time, despite the crucial role of Au adatoms in on-surface reactions,[45−47] the exact role of Au adatoms is generally difficult to experimentally discriminate on

Au(111)[45,46] as they are always available at or above RT. Thus, we believe that the Au(111) substrate (including Au adatoms) should also play an important role in the whole reaction processes. Nevertheless, with the presence of Au adatoms in all of the cases shown above, the introduction of Na atoms has been demonstrated to both isolate the dissociated halogens and facilitate the C−Br activation under mild conditions compared to the Na-free cases, confirming it to be the dominant effect.

Furthermore, considering the three following aspects, (1) the highly programmable characteristics and wide applications of Ullmann-type dehalogenative coupling reactions in the field of on-surface synthesis, (2) the fact that dissociated halogens chemisorbed on Au(111) usually impede the diffusion of dehalogenated radicals via a reversible recombination,[11,43] prohibit the generation of longer polymers,[44] and interfere with the property characterization,[30,48,49] and (3) the difficulties in both eliminating dissociated halogens and reducing reaction barriers using the previously reported strategies, it is of great value to develop an alternative strategy to overcome these drawbacks and is thus significant for the atomically precise structural construction and accurate property characterization.

CONCLUSIONS

In conclusion, we have successfully developed a halogen separation strategy for dehalogenative reactions on Au(111) by introducing extrinsic Na atoms into molecular systems and demonstrated its versatility in both intermolecular halogen isolation and facilitation of intramolecular C−Br activation. Based on the model systems of the DBIBP molecule and the more general DBTP molecule, the combination of STM imaging and DFT calculations has experimentally and theoretically verified that this strategy is able to isolate free halogens by forming NaX islands and to promote the C−Br activation by lowering the reaction temperatures/barriers as well as by separating dissociated halogens from the reaction systems. Thus, Na-induced C−Br activation is feasible under mild conditions. Such an effective halogen separation strategy should be promising in reducing the influence of halogen byproducts and significant for dehalogenation-based programmed structure construction and accurate property characterization.

METHODS

The STM experiments were performed in an ultrahigh-vacuum (UHV) chamber with a base pressure of 1×10^{-10} mbar equipped with a variable-temperature "Aarhus-type" STM from SPECS.[50,51] The Au(111) substrate was cleaned by Ar^+-ion sputtering and annealing at ∼800 K for repeated cycles. Two separate homemade molecular evaporators were used for the sample preparation. After thorough degassing, the DBIBP and DBTP molecules (purchased from Bidepharm and Adamas, with purities greater than 95% and 98%, respectively) were evaporated by thermal sublimation at ∼345 and ∼447 K, respectively, onto a clean Au(111) substrate held at room temperature (RT, ∼300 K). The pure sodium (Na, from SAES Getters) was dosed through conventional resistance heating of a wire-type Na dispenser after complete degassing. The amount of Na was calibrated and defined by applying a constant current (∼6.5 A) for a time interval of 1.5 min once, and more Na was introduced by gradually increasing the number of deposition times. The sodium halides (NaI and NaBr, purchased from Sigma-Aldrich, with a purity greater than 99%) were also evaporated by thermal sublimation. The sample was thereafter transferred within the UHV chamber to the STM head for scanning. Typical scanning conditions: $V = -1.2$ V and $I = 0.5-0.8$ nA. All the STM images were recorded in a typical temperature range of 100−150 K and were further smoothed to eliminate noises.

The calculations were performed in the framework of DFT by using the Vienna ab initio simulation package (VASP).[52,53] The projector-augmented wave method was used to describe the interaction between ions and electrons.[54,55] The Perdew−Burke−Ernzerhof generalized gradient approximation exchange-correlation functional was employed,[56] and van der Waals interactions were included using the dispersion-corrected DFT-D3 method of Grimme.[57] The atomic structures were relaxed using the conjugate gradient algorithm scheme as implemented in the VASP code until the forces on all unconstrained atoms were ≤0.03 eV/Å. Plane waves were used as a basis set with an energy cutoff of 400 eV. The simulated STM images were obtained by using the Tersoff−Hamann method,[58] in which the local density of states (LDOS) is used to approximate the tunneling current. The Au(111) substrates were modeled by a three-layered slab separated by an ∼15 Å vacuum region for the structural models, where the bottom layer was fixed. Transition states were searched by the climbing image nudged elastic band (CI-NEB)[59] and dimer methods,[60] and all the local minima and saddle points were optimized until the forces on all unconstrained atoms were ≤0.03 eV/Å.

ASSOCIATED CONTENT

Supporting Information

The Supporting Information is available free of charge at https://pubs.acs.org/doi/10.1021/acsnano.3c12949.

Supplementary STM images and DFT calculations (PDF)

AUTHOR INFORMATION

Corresponding Authors

Chi Zhang − *Interdisciplinary Materials Research Center, School of Materials Science and Engineering, Tongji University, Shanghai 201804, People's Republic of China*; Email: zhangchi11@tongji.edu.cn

Wei Xu − *Interdisciplinary Materials Research Center, School of Materials Science and Engineering, Tongji University, Shanghai 201804, People's Republic of China*; orcid.org/0000-0003-0216-794X; Email: xuwei@tongji.edu.cn

Authors

Zhaoyu Zhang − *Interdisciplinary Materials Research Center, School of Materials Science and Engineering, Tongji University, Shanghai 201804, People's Republic of China*

Yuhong Gao − *Interdisciplinary Materials Research Center, School of Materials Science and Engineering, Tongji University, Shanghai 201804, People's Republic of China*

Zewei Yi − *Interdisciplinary Materials Research Center, School of Materials Science and Engineering, Tongji University, Shanghai 201804, People's Republic of China*

Complete contact information is available at: https://pubs.acs.org/10.1021/acsnano.3c12949

Author Contributions

The manuscript was written through contributions of all authors. All authors have given approval to the final version of the manuscript.

Notes

The authors declare no competing financial interest.

ACKNOWLEDGMENTS

The authors acknowledge financial support from the Ministry of Science and Technology of the People's Republic of China (2023YFE0101900), the National Natural Science Foundation of China (Grants Nos. 22202153, 22125203, and 21790351), and the Fundamental Research Funds for the Central Universities. The authors are grateful for the use of RIKEN's HOKUSAI supercomputer system. The authors are also grateful for the fruitful discussion with Dr. Yuanqi Ding.

REFERENCES

(1) Grill, L.; Hecht, S. Covalent On-Surface Polymerization. *Nat. Chem.* **2020**, *12*, 115−130.

(2) Talirz, L.; Ruffieux, P.; Fasel, R. On-Surface Synthesis of Atomically Precise Graphene Nanoribbons. *Adv. Mater.* **2016**, *28*, 6222−6231.

(3) Clair, S.; de Oteyza, D. G. Controlling a Chemical Coupling Reaction on a Surface: Tools and Strategies for On-Surface Synthesis. *Chem. Rev.* **2019**, *119*, 4717−4776.

(4) Fan, Q.; Gottfried, J. M.; Zhu, J. Surface-Catalyzed C-C Covalent Coupling Strategies toward the Synthesis of Low-Dimensional Carbon-Based Nanostructures. *Acc. Chem. Res.* **2015**, *48*, 2484−2494.

(5) Zhang, C.; Yi, Z.; Xu, W. Scanning Probe Microscopy in Probing Low-Dimensional Carbon-Based Nanostructures and Nanomaterials. *Mater. Futures* **2022**, *1*, 032301.

(6) Grill, L.; Dyer, M.; Lafferentz, L.; Persson, M.; Peters, M. V.; Hecht, S. Nano-Architectures by Covalent Assembly of Molecular Building Blocks. *Nat. Nanotechnol.* **2007**, *2*, 687−691.

(7) Cai, J.; Ruffieux, P.; Jaafar, R.; Bieri, M.; Braun, T.; Blankenburg, S.; Muoth, M.; Seitsonen, A. P.; Saleh, M.; Feng, X.; et al. Atomically Precise Bottom-Up Fabrication of Graphene Nanoribbons. *Nature* **2010**, *466*, 470−473.

(8) Fan, Q.; Martin-Jimenez, D.; Werner, S.; Ebeling, D.; Koehler, T.; Vollgraff, T.; Sundermeyer, J.; Hieringer, W.; Schirmeisen, A.; Gottfried, J. M. On-Surface Synthesis and Characterization of a Cycloarene: C108 Graphene Ring. *J. Am. Chem. Soc.* **2020**, *142*, 894−899.

(9) Zhang, C.; Kazuma, E.; Kim, Y. Atomic-Scale Visualization of the Stepwise Metal-Mediated Dehalogenative Cycloaddition Reaction Pathways: Competition between Radicals and Organometallic Intermediates. *Angew. Chem., Int. Ed.* **2019**, *58*, 17736−17744.

(10) Björk, J.; Hanke, F.; Stafström, S. Mechanisms of Halogen-Based Covalent Self-Assembly on Metal Surfaces. *J. Am. Chem. Soc.* **2013**, *135*, 5768−5775.

(11) Batra, A.; Cvetko, D.; Kladnik, G.; Adak, O.; Cardoso, C.; Ferretti, A.; Prezzi, D.; Molinari, E.; Morgante, A.; Venkataraman, L. Probing the Mechanism for Graphene Nanoribbon Formation on Gold Surfaces through X-Ray Spectroscopy. *Chem. Sci.* **2014**, *5*, 4419−4423.

(12) Fritton, M.; Duncan, D. A.; Deimel, P. S.; Rastgoo-Lahrood, A.; Allegretti, F.; Barth, J. V.; Heckl, W. M.; Björk, J.; Lackinger, M. The Role of Kinetics versus Thermodynamics in Surface-Assisted Ullmann Coupling on Gold and Silver Surfaces. *J. Am. Chem. Soc.* **2019**, *141*, 4824−4832.

(13) Abyazisani, M.; MacLeod, J. M.; Lipton-Duffin, J. Cleaning up after the Party: Removing the Byproducts of On-Surface Ullmann Coupling. *ACS Nano* **2019**, *13*, 9270−9278.

(14) Zuzak, R.; Jančařík, A.; Gourdon, A.; Szymonski, M.; Godlewski, S. On-Surface Synthesis with Atomic Hydrogen. *ACS Nano* **2020**, *14*, 13316−13323.

(15) Sun, K.; Nishiuchi, T.; Sahara, K.; Kubo, T.; Foster, A. S.; Kawai, S. Low-Temperature Removal of Dissociated Bromine by Silicon Atoms for an On-Surface Ullmann Reaction. *J. Phys. Chem. C* **2020**, *124*, 19675−19680.

(16) Enderson, Z. A.; Murali, H.; Dasari, R. R.; Dai, Q.; Li, H.; Parker, T. C.; Brédas, J.-L.; Marder, S. R.; First, P. N. Tailoring On-Surface Molecular Reactions and Assembly through Hydrogen-Modified Synthesis: From Triarylamine Monomer to 2D Covalent Organic Framework. *ACS Nano* **2023**, *17*, 7366−7376.

(17) Sun, K.; Silveira, O. J.; Ma, Y.; Hasegawa, Y.; Matsumoto, M.; Kera, S.; Krejčí, O.; Foster, A. S.; Kawai, S. On-Surface Synthesis of Disilabenzene-Bridged Covalent Organic Frameworks. *Nat. Chem.* **2023**, *15*, 136−142.

(18) Lin, T.; Shang, X. S.; Adisoejoso, J.; Liu, P. N.; Lin, N. Steering On-Surface Polymerization with Metal-Directed Template. *J. Am. Chem. Soc.* **2013**, *135*, 3576−3582.

(19) Adisoejoso, J.; Lin, T.; Shang, X. S.; Shi, K. J.; Gupta, A.; Liu, P. N.; Lin, N. A Single-Molecule-Level Mechanistic Study of Pd-Catalyzed and Cu-Catalyzed Homocoupling of Aryl Bromide on an Au(111) Surface. *Chem.-Eur. J.* **2014**, *20*, 4111−4116.

(20) Xing, S.; Liu, B.; Wang, W.; Guo, J.; Wang, W. On-Surface Synthesis of Graphene Nanoribbons Catalyzed by Ni Atoms. *Chem.-Asian J.* **2018**, *13*, 2023−2026.

(21) Cirera, B.; Björk, J.; Otero, R.; Gallego, J. M.; Miranda, R.; Ecija, D. Efficient Lanthanide Catalyzed Debromination and Oligomeric Length-Controlled Ullmann Coupling of Aryl Halides. *J. Phys. Chem. C* **2017**, *121*, 8033−8041.

(22) Feng, L.; Wang, T.; Jia, H.; Huang, J.; Han, D.; Zhang, W.; Ding, H.; Xu, Q.; Du, P.; Zhu, J. On-Surface Synthesis of Planar Acenes via Regioselective Aryl-Aryl Coupling. *Chem. Commun.* **2020**, *56*, 4890−4893.

(23) Zhang, H.; Franke, J.-H.; Zhong, D.; Li, Y.; Timmer, A.; Arado, O. D.; Mönig, H.; Wang, H.; Chi, L.; Wang, Z.; et al. Surface Supported Gold-Organic Hybrids: On-Surface Synthesis and Surface Directed Orientation. *Small* **2014**, *10*, 1361−1368.

(24) Liu, M.; Liu, M.; She, L.; Zha, Z.; Pan, J.; Li, S.; Li, T.; He, Y.; Cai, Z.; Wang, J.; et al. Graphene-Like Nanoribbons Periodically Embedded with Four- and Eight-Membered Rings. *Nat. Commun.* **2017**, *8*, 14924.

(25) Lafferentz, L.; Eberhardt, V.; Dri, C.; Africh, C.; Comelli, G.; Esch, F.; Hecht, S.; Grill, L. Controlling On-Surface Polymerization by Hierarchical and Substrate-Directed Growth. *Nat. Chem.* **2012**, *4*, 215−220.

(26) Zhong, Q.; Niu, K.; Chen, L.; Zhang, H.; Ebeling, D.; Björk, J.; Müllen, K.; Schirmeisen, A.; Chi, L. Substrate-Modulated Synthesis of Metal-Organic Hybrids by Tunable Multiple Aryl-Metal Bonds. *J. Am. Chem. Soc.* **2022**, *144*, 8214−8222.

(27) Gao, Y.; Zhang, Z.; Yi, Z.; Zhang, C.; Xu, W. Visualizing the Hierarchical Evolution of Aryl-Metal Bonding in Organometallic Nanostructures on Ag(111). *J. Phys. Chem. Lett.* **2023**, *14*, 10819−10824.

(28) Jang, W. J.; Chung, K.-H.; Lee, M. W.; Kim, H.; Lee, S.; Kahng, S.-J. Tetragonal Porous Networks Made by Rod-Like Molecules on Au(111) with Halogen Bonds. *Appl. Surf. Sci.* **2014**, *309*, 74−78.

(29) Shang, J.; Wang, Y.; Chen, M.; Dai, J.; Zhou, X.; Kuttner, J.; Hilt, G.; Shao, X.; Gottfried, J. M.; Wu, K. Assembling Molecular Sierpiński Triangle Fractals. *Nat. Chem.* **2015**, *7*, 389−393.

(30) Kawai, S.; Takahashi, K.; Ito, S.; Pawlak, R.; Meier, T.; Spijker, P.; Canova, F. F.; Tracey, J.; Nozaki, K.; Foster, A. S.; et al. Competing Annulene and Radialene Structures in a Single Anti-Aromatic Molecule Studied by High-Resolution Atomic Force Microscopy. *ACS Nano* **2017**, *11*, 8122−8130.

(31) Xie, L.; Zhang, C.; Ding, Y.; Xu, W. Structural Transformation and Stabilization of Metal-Organic Motifs Induced by Halogen Doping. *Angew. Chem., Int. Ed.* **2017**, *56*, 5077−5081.

(32) Jiménez-Martín, A.; Gallardo, A.; de la Torre, B. Coverage-Modulated Halogen Bond Geometry Transformation in Supramolecular Assemblies. *Nanoscale* **2023**, *15*, 16354−16361.

(33) Hou, R.; Guo, Y.; Yi, Z.; Zhang, Z.; Zhang, C.; Xu, W. Construction and Structural Transformation of Metal-Organic Nanostructures Induced by Alkali Metals and Alkali Metal Salts. *J. Phys. Chem. Lett.* **2023**, *14*, 3636−3642.

(34) Lin, Y.; Huang, Z.; Wen, X.; Rong, W.; Peng, Z.; Diao, M.; Xing, L.; Dai, J.; Zhou, X.; Wu, K. Steering Effect of Bromine on

Intermolecular Dehydrogenation Coupling of Poly(p-phenylene) on Cu(111). *ACS Nano* **2020**, *14*, 17134−17141.

(35) Yi, Z.; Zhang, C.; Zhang, Z.; Hou, R.; Guo, Y.; Xu, W. On-Surface Synthesis of Na-Porphyrins Using NaCl as a Convenient Na Source. *Precis. Chem.* **2023**, *1*, 226−232.

(36) Yi, Z.; Guo, Y.; Hou, R.; Zhang, Z.; Gao, Y.; Zhang, C.; Xu, W. Revealing the Orientation Selectivity of Tetrapyridyl-Substituted Porphyrins Constrained in Molecular "Klotski Puzzles". *J. Am. Chem. Soc.* **2023**, *145*, 22366−22373.

(37) Dai, J.; Zhao, X.; Peng, Z.; Li, J.; Lin, Y.; Wen, X.; Xing, L.; Zhao, W.; Shang, J.; Wang, Y.; et al. Assembling Surface Molecular Sierpiński Triangle Fractals via K^+-Invoked Electrostatic Interaction. *J. Am. Chem. Soc.* **2023**, *145*, 13531−13536.

(38) Shan, H.; Zhou, L.; Ji, W.; Zhao, A. Flexible Alkali-Halogen Bonding in Two Dimensional Alkali-Metal Organic Frameworks. *J. Phys. Chem. Lett.* **2021**, *12*, 10808−10814.

(39) Berdonces-Layunta, A.; Schulz, F.; Aguilar-Galindo, F.; Lawrence, J.; Mohammed, M. S. G.; Muntwiler, M.; Lobo-Checa, J.; Liljeroth, P.; de Oteyza, D. G. Order from a Mess: The Growth of 5-Armchair Graphene Nanoribbons. *ACS Nano* **2021**, *15*, 16552−16561.

(40) Galeotti, G.; De Marchi, F.; Taerum, T.; Besteiro, L. V.; El Garah, M.; Lipton-Duffin, J.; Ebrahimi, M.; Perepichka, D. F.; Rosei, F. Surface-Mediated Assembly, Polymerization and Degradation of Thiophene-Based Monomers. *Chem. Sci.* **2019**, *10*, 5167−5175.

(41) Qin, T.; Guo, D.; Xiong, J.; Li, X.; Hu, L.; Yang, W.; Chen, Z.; Wu, Y.; Ding, H.; Hu, J.; et al. Synthesis of a Porous [14]Annulene Graphene Nanoribbon and a Porous [30]Annulene Graphene Nanosheet on Metal Surfaces. *Angew. Chem., Int. Ed.* **2023**, *62*, No. e202306368.

(42) Merino-Díez, N.; Pérez Paz, A.; Li, J.; Vilas-Varela, M.; Lawrence, J.; Mohammed, M. S. G.; Berdonces-Layunta, A.; Barragán, A.; Pascual, J. I.; Lobo-Checa, J.; et al. Hierarchy in the Halogen Activation During Surface-Promoted Ullmann Coupling. *ChemPhysChem* **2019**, *20*, 2305−2310.

(43) Stolz, S.; Di Giovannantonio, M.; Urgel, J. I.; Sun, Q.; Kinikar, A.; Borin Barin, G.; Bommert, M.; Fasel, R.; Widmer, R. Reversible Dehalogenation in On-Surface Aryl-Aryl Coupling. *Angew. Chem., Int. Ed.* **2020**, *59*, 14106−14110.

(44) Di Giovannantonio, M.; Deniz, O.; Urgel, J. I.; Widmer, R.; Dienel, T.; Stolz, S.; Sánchez-Sánchez, C.; Muntwiler, M.; Dumslaff, T.; Berger, R.; et al. On-Surface Growth Dynamics of Graphene Nanoribbons: The Role of Halogen Functionalization. *ACS Nano* **2018**, *12*, 74−81.

(45) Lowe, B.; Hellerstedt, J.; Matěj, A.; Mutombo, P.; Kumar, D.; Ondráček, M.; Jelinek, P.; Schiffrin, A. Selective Activation of Aromatic C-H Bonds Catalyzed by Single Gold Atoms at Room Temperature. *J. Am. Chem. Soc.* **2022**, *144*, 21389−21397.

(46) Björk, J.; Sánchez-Sánchez, C.; Chen, Q.; Pignedoli, C. A.; Rosen, J.; Ruffieux, P.; Feng, X.; Narita, A.; Müllen, K.; Fasel, R. The Role of Metal Adatoms in a Surface-Assisted Cyclodehydrogenation Reaction on a Gold Surface. *Angew. Chem., Int. Ed.* **2022**, *61*, No. e202212354.

(47) Zhang, Z.; Perepichka, D. F.; Khaliullin, R. Z. Adatoms in the Surface-Confined Ullmann Coupling of Phenyl Groups. *J. Phys. Chem. Lett.* **2021**, *12*, 11061−11069.

(48) Rastgoo-Lahrood, A.; Lischka, M.; Eichhorn, J.; Samanta, D.; Schmittel, M.; Heckl, W. M.; Lackinger, M. Reversible Intercalation of Iodine Monolayers between On-Surface Synthesised Covalent Polyphenylene Networks and Au(111). *Nanoscale* **2017**, *9*, 4995−5001.

(49) Rastgoo-Lahrood, A.; Björk, J.; Lischka, M.; Eichhorn, J.; Kloft, S.; Fritton, M.; Strunskus, T.; Samanta, D.; Schmittel, M.; Heckl, W. M.; et al. Post-Synthetic Decoupling of On-Surface-Synthesized Covalent Nanostructures from Ag(111). *Angew. Chem., Int. Ed.* **2016**, *55*, 7650−7654.

(50) Besenbacher, F. Scanning Tunnelling Microscopy Studies of Metal Surfaces. *Rep. Prog. Phys.* **1996**, *59*, 1737−1802.

(51) Laegsgaard, E.; Österlund, L.; Thostrup, P.; Rasmussen, P. B.; Stensgaard, I.; Besenbacher, F. A High-Pressure Scanning Tunneling Microscope. *Rev. Sci. Instrum.* **2001**, *72*, 3537−3542.

(52) Kresse, G.; Hafner, J. *Ab Initio* Molecular Dynamics for Open-Shell Transition Metals. *Phys. Rev. B* **1993**, *48*, 13115−13118.

(53) Kresse, G.; Furthmüller, J. Efficient Iterative Schemes for *Ab Initio* Total-Energy Calculations Using a Plane-Wave Basis Set. *Phys. Rev. B* **1996**, *54*, 11169−11186.

(54) Blöchl, P. E. Projector Augmented-Wave Method. *Phys. Rev. B* **1994**, *50*, 17953−17979.

(55) Kresse, G.; Joubert, D. From Ultrasoft Pseudopotentials to the Projector Augmented-Wave Method. *Phys. Rev. B* **1999**, *59*, 1758−1775.

(56) Perdew, J. P.; Burke, K.; Ernzerhof, M. Generalized Gradient Approximation Made Simple. *Phys. Rev. Lett.* **1996**, *77*, 3865−3868.

(57) Grimme, S.; Antony, J.; Ehrlich, S.; Krieg, H. A Consistent and Accurate *Ab Initio* Parametrization of Density Functional Dispersion Correction (DFT-D) for the 94 Elements H-Pu. *J. Chem. Phys.* **2010**, *132*, 154104.

(58) Tersoff, J.; Hamann, D. R. Theory of the Scanning Tunneling Microscope. *Phys. Rev. B* **1985**, *31*, 805−813.

(59) Henkelman, G.; Uberuaga, B. P.; Jónsson, H. A Climbing Image Nudged Elastic Band Method for Finding Saddle Points and Minimum Energy Paths. *J. Chem. Phys.* **2000**, *113*, 9901−9904.

(60) Kästner, J.; Sherwood, P. Superlinearly Converging Dimer Method for Transition State Search. *J. Chem. Phys.* **2008**, *128*, 014106.